

# A Nanosensor Platform for Biologging in Marine Animals

Xiaojia Jin<sup>1</sup>, Ali A. Alizadehmojarad<sup>1</sup>, Volodymyr B. Koman<sup>1</sup>, Gabriel Sánchez-Velázquez<sup>1</sup>, Manki Son<sup>1</sup>, Rory Wilson<sup>2</sup>, Mark Meekan<sup>3</sup>, Carlos M. Duarte<sup>4</sup>, and Michael S. Strano<sup>1,\*</sup>

<sup>1</sup>77 Massachusetts Ave., Department of Chemical Engineering, Massachusetts Institute of Technology, Cambridge, MA, 02139, USA

<sup>2</sup>Biosciences, College of Science, Swansea University, Singleton Park, Swansea SA2 8PP, United Kingdom

<sup>3</sup>Australian Institute of Marine Science, the Indian Ocean Marine Research Centre (IOMRC), The University of Western Australia (M470), 35 Stirling Highway, 6009 Perth, Australia

<sup>4</sup>Red Sea Research Center, Division of Biological and Environmental Sciences and Engineering, King Abdullah University of Science and Technology, Thuwal 23955-6900, Saudi Arabia

Corresponding author's email address: strano@mit.edu

**KEYWORDS** *tagging, nanosensor, biologging, biochemical monitoring, steroid sensing*

**ABSTRACT:** Biologging has significantly advanced ecological biology by enabling the collection of data from free-roaming animals in their natural habitats. Traditionally, these measurements have largely been limited to temperature, pressure, and movement. Incorporating physiological data of animal biomarkers could yield valuable orthogonal datasets, providing a more nuanced understanding of organisms in the context of their environments and behaviors. Despite this potential, successful collection of such biochemical information remains absent, and thus motivates new sensor platforms. Towards this end, we explore the hardware and nanosensor optimization of animal implantable sensors for tracking hormone levels in marine animals. The transducer element is based on polymer-wrapped single-walled carbon nanotubes (SWCNT) that act as nanosensors embedded within a biocompatible poly (ethylene glycol) diacrylate (PEGDA) hydrogel. This work investigates the performance of the nanosensor hydrogel under various temperatures, illumination conditions, and nanoparticle concentration in the hydrogel. We further prototype a miniaturized fluorescent system for integration into existing, commercially available acoustic tags widely used in marine biology studies. We demonstrate a baseline of 100 nM for the detection limit of progesterone as an example of an important hormone in marine animals, using the integrated nanosensor hydrogel in this platform. Further improvement is possible with optimization of the signal to noise via hardware development. This developed form-factor will complement the presently collected data by providing insights into the physiological state of the animals in the context of their behavior and environments.

Marine animals undertake extensive migrations, traversing vast distances and sometimes entire ocean basins, which pose significant challenges for direct observation and monitoring of their behaviors and environments.<sup>1,2</sup> To overcome these challenges, researchers have developed bio-logging techniques, also known as animal telemetry, biotelemetry, or animal-borne sensors.<sup>3-5</sup> These methods involve equipping animals with miniaturized tags to log and/or relay data relevant to marine ecology. Bio-logging has become a cornerstone in the study of marine animals, offering the opportunity to observe the physical and biological environment through which these animals travel, enhancing our understanding of their ecology.<sup>5,6</sup> This technology provides insight into how animals interact with human activities<sup>1</sup> and informs target conservation efforts.<sup>7</sup>

In recent years, marine biologging has witnessed significant advancements, revolutionizing our understanding of marine ecosystems and species behaviors.<sup>2</sup> By attaching various tracking devices to marine animals, researchers

have been able to collect valuable data on their movements, foraging patterns,<sup>8</sup> migration routes,<sup>9,10</sup> and even physiological parameters.<sup>9,11</sup> For instances, satellite tags have been used to track the migration patterns and habitat use of sharks,<sup>12-14</sup> while accelerometers attached to fish have provided data on their swimming behavior and energy expenditure.<sup>15,16</sup>

One key area of development in marine biologging is the miniaturization of tracking devices.<sup>3</sup> Advances in technology have allowed for the development of smaller, lighter, and more sophisticated tags that can be attached to a wide range of marine organisms, including fish, mammals, birds, and even invertebrates.<sup>17,18</sup> These tags often incorporate satellite or acoustic telemetry, global positioning system (GPS),<sup>19</sup> accelerometers,<sup>20</sup> and sensors for measuring environmental parameters, such as temperature and salinity.<sup>21</sup> Additionally, a significant development has been the integration of biologging data with other sources of information, such as remote sensing and oceanographic datasets.<sup>2</sup> By combining these datasets,

researchers can gain a more comprehensive understanding of the ecological processes and environmental factors that influencing marine animal behavior. Such integrated approaches have led to breakthroughs in our knowledge of marine food webs, species interactions, and the impacts of environmental changes on marine ecosystems.

Despite the significant advancements in marine biogging, measurements have predominantly focused on physical parameters like temperature, pressure, and movement.<sup>22,23</sup> The ability to monitor biochemical markers in freely moving marine animals remains underdeveloped.<sup>24,25</sup> Gaining access to such biochemical data would provide valuable orthogonal datasets and enable a more nuanced understanding of their physiology, behavior, and environmental interactions. One category of chemicals of significant importance is steroid hormones.<sup>26</sup> Steroid hormones play a pivotal role in the physiological processes of marine animals, including sex determination, sex change, and stress response.<sup>27,28</sup> Some species of fish, for instance, may change their sex from male to female, disrupting the balance for optimal breeding and reproduction. Both genotypic (GSD) and temperature-dependent (TSD) sex determination mechanisms exist, with warmer water temperatures during early development potentially yielding more males.<sup>29</sup> Moreover, sex change may occur later in life as a consequence of reproductive potential relative to local social pressures.<sup>30</sup> Physiologically, steroids, such as estrogens and androgens, as well as aromatase inhibitors, have been implicated in sex changes.<sup>31</sup> In addition to sex-related processes, aquatic organisms become more susceptible to disease and stunted growth during periods of high stress, which manifests itself in higher endogenous cortisol levels.<sup>32</sup> The activity of estrogens and androgens in the case of sex change and cortisol in the case of stress provide valuable metrics for assessing the conditions of marine animals. Additionally, progesterone levels in marine organisms have been the focus of growing research because they can reveal reproductive events and indicate maturity, both of which provide insights into population demographics.<sup>33–35</sup>

The problem of continuous biochemical monitoring in marine animals is associated with several challenges, including (1) residual movement of a sensor with respect to tissue causing measurement artefacts, (2) sensitive and selective detection, and (3) long-term stability.<sup>2,36</sup> While various sensor types like electrochemical,<sup>37</sup> and fluorophore-based sensors<sup>38</sup> have been explored for biochemical sensing, none have successfully enabled real-time *in vivo* monitoring in freely swimming marine animals. In recent years, single-walled carbon nanotubes (SWCNTs) have emerged as promising candidates for *in vivo* sensing, offering advantages of photostability and near-infrared (nIR) fluorescence, which allows for deep tissue penetration.<sup>39,40</sup> Our group has previously developed SWCNT-based nanosensors for detecting various analytes including neurotransmitters,<sup>41,42</sup> proteins,<sup>43,44</sup> and hormones.<sup>45</sup> Building on this work, we now aim to integrate SWCNT nanosensors into implantable devices for marine animals, with a specific focus on monitoring progesterone levels as

an example of a steroid hormone of interest. Specifically, progesterone levels in marine organisms have been the focus of growing research because they can reveal reproductive events and indicate maturity, both of which provide insights into population demographics.<sup>33–35</sup>

Herein, we present the development and optimization of a miniaturized, implantable biogging tag with an integrated SWCNT nanosensor for the continuous monitoring of progesterone in marine animals. Marine organisms contain several steroid hormones that may interfere with the detection of progesterone, the hormone of interest in this study. Key interfering hormones include testosterone, estradiol, and cortisol. Although the physiological level of these steroids is almost in the same range, we previously developed a sensor with specific detection of progesterone against a panel of steroid hormones.<sup>42</sup> The tag is engineered to meet the size and power constraints of existing commercial fish tags. We have systematically characterized the nanosensor performance in a custom hydrogel matrix under varying conditions. Integration of the sensor and electronic components into a compact tag design (**Fig. 1**) is accompanied by the development of an analytical model to enhance and guide tag optimization. As a proof-of-concept, we demonstrate sensitive, stable, and reversible progesterone detection under simulated conditions. This SWCNT nanosensor-enabled tag provides an unprecedented platform for continuous *in vivo* biochemical monitoring in marine animals. The ability to collect this new class of data will facilitate more holistic biogging studies to decipher the complex interplay between animal physiology, behavior, and the environment. Ultimately, such advances in marine biogging can inform data-driven decision making in marine conservation and sustainable aquaculture.

The SWCNT nanosensor and the supporting optoelectronic components (**Fig. 1b–c**) are designed to be located at the tip of an existing tag (**Fig. 1d**), enabling modular architecture. The optoelectronic system is composed of a light-emitting diode (LED) and a detector. The LED may be powered by a tag, whereas the detector may transmit the acquired data into tag's memory. The optoelectronic components are separated from the environments using an insulating yet optically transparent protective window. The window and a capping system sandwich a sensing hydrogel that is directly exposed to a local environment, enabling unobscured chemical access of sensing species to nanosensors.

## EXPERIMENTAL SECTION

**Materials.** Raw single walled carbon nanotubes (SWCNT) produced from the High-Pressure Carbon Monoxide (HiPCO) process were purchased from NanoIntegris and used without further processing (Batch HR27-104). Poly (ethylene glycol) diacrylate (PEGDA) (Mn = 10000, Mn = 8000, Mn = 6000) were purchased from Alfa Aesar. All other materials were purchased from Sigma-Aldrich.

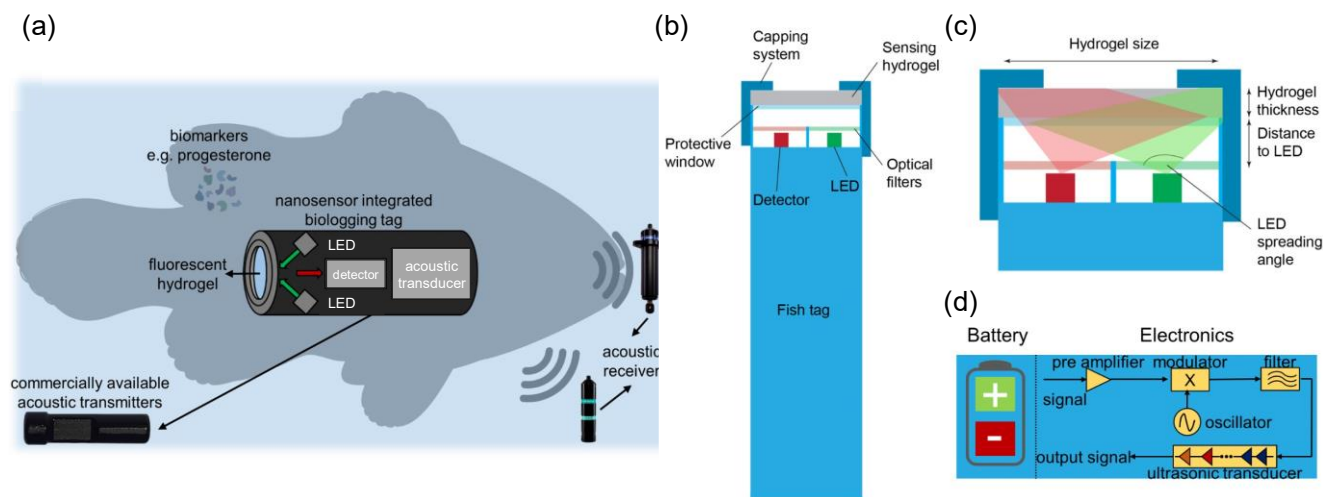


**Figure 1.** Vision for future biologging, where biochemical sensors are integrated onto existing tags for biologging providing an orthogonal set of data for studying the ecology system. (a) A concept of a biologging tag to be used into marine animals with wireless communication. The tag is comprised of an implantable acoustic telemetry tag, hydrogel carbon nanotube sensors, optical components for the readout, and electronic components for signal transmission to shore stations. (b) A schematic of the optical component with a protective cap for nanosensor clamping in the form of biocompatible hydrogel. (c) An optical system for detecting signals from nanosensors is comprised of an excitation LED, a detector, and optimally positioned optical filters. (d) An acoustic transmitter comprised of a battery and electronic components that convert acoustic signal to digital data.

**Cortisol acrylation.** Acrylation of cortisol was carried out in accordance with the methods described by Lee et al.<sup>45</sup> Briefly, 2g cortisol and 850mL trimethylamine (TEA) were dissolved in 50mL tetrahydrofuran (THF). The solution was then placed in an ice-bath with magnetic stirring, followed by dropwise addition of acryloyl chloride (0.5mL) diluted in THF (10 vol%). The reaction mixture was placed in ice-bath for 1h and proceeded at room temperature for 2d. After completion of the reaction, the solution was decanted from the hydrogen chloride (HCl)-TEA salts, and THF was removed by rotary evaporation.

The product was reconstituted in 50mL dichloromethane (DCM), followed by three times of HCl (0.5 M) wash, two times of NaHCO<sub>3</sub> (5 wt%) wash, and one time of saturated aqueous NaCl wash. The solution was then dried using anhydrous Na<sub>2</sub>SO<sub>4</sub>. The structure of the product was confirmed using <sup>1</sup>H NMR (Bruker AVANCE III-400 NMR Spectrometer).

**Polymer synthesis.** Polymer synthesis was done as described previously.<sup>45</sup> Briefly, styrene (742μL), acrylic acid (1900μL) and acrylated cortisol (385mg) monomers were dissolved in 10mL of 1,4-dioxane. Hydroquinone monomethyl ether (MEHQ) was removed acrylic acid by passing through a column packed with inhibitor removers. Similarly, 4-tert-butylcatechol was removed from styrene. 2-(Dedecylthiocarbonothioylthio)-2-methylpropionic acid (67.5mg, 1 equiv.) and 2,2'-azobis (2-methylpropionitrile) (6.08mg, 0.2 equiv.) were added to the reaction mixture. The solution was purged with N<sub>2</sub> for 30mins, and the reaction was proceeded in nitrogen environment at 70 °C for 24hrs. The mixture was precipitated in 300mL diethyl ether afterwards. The unreacted monomer was removed by reconstituting the product in THF and re-precipitating in diethyl ether twice. The polymer was dried under vac-

uum for 3d and characterized using <sup>1</sup>H NMR (Bruker AVANCE III-400 NMR Spectrometer).

**Polymer SWCNT dispersion.** 5 mg of HiPCO SWCNT and 50 mg of polymer were mixed in 5mL of PBS. The solution was adjusted to a final pH of 7.4 by dropwise addition of 2M NaOH. The mixture was bath sonicated for 10min and ultrasonicated using a 6 mm probe at a power of 10W for 1h (QSonica). The resulting suspension was ultracentrifuged at 155000 rcf for 4hr. The supernatant (top 80%) was collected for future use and free polymer was removed from the suspension by dialysis against 1X PBS over 5 days using 100 kDa cutoff Float-a-Lyzer devices (Spectrum Labs). The dialysis buffer was replaced thrice daily. UV-Vis-nIR absorption spectroscopy (Shimadzu 3101PC) was used to verify the presence of the characteristic absorption peaks for SWCNTs. The concentration of the final suspension was determined using the absorption at 632 nm with an extinction coefficient of  $\epsilon_{632} = 0.036 \text{ mg(L cm)}^{-1}$ .<sup>46</sup>

**Near-infrared fluorescent spectra measurements.** The nIR emission spectra of the polymer-SWCNT suspension was measured using a nIR customized microscope, which consists of a Zeiss Axio Vision inverted microscope body with a 20X objective, coupled to an Acton SP2500 spectrometer and liquid nitrogen cooled indium gallium arsenide (InGaAs) 1D detector (Princeton Instruments). In a 96-well plate, the SWCNT dispersion (1mg/L) were mixed with progesterone (100μM) to a final volume of 200 μL in 1X PBS with 2 vol% DMSO. The spectral control is made of similar aqueous solution without nanotubes. Following incubation for 1hr on a tabletop shaker, the samples were illuminated by a 150 mW 785 nm photodiode laser (B&W Tek Inc.), and the fluorescent emission spectra were collected from 950 to 1250nm.

**Hydrogel synthesis.** SWCNT were encapsulated in a hydrogel matrix using a modified version of a previously reported protocol.<sup>45</sup> Briefly, PEGDA (100mg/L), SWCNT dispersion (10mg/L), and 2-hydroxy-4'-(2-hydroxyethoxy)-2-methylpropiophenone (0.175mg/L) were mixed in 1X PBS. The mixture was placed into a customized mold, and purged with N<sub>2</sub> for 30 mins. The solution was exposed to UV light source (Cure Spot 50, Dymax Corp) protected by OD 1.5 filter with a final illumination intensity of 23 mW/cm<sup>2</sup> for 8 min to polymerize and form the hydrogels. After polymerization, the hydrogels were incubated in 1X PBS to equilibrate for 48 h before testing.

**Standoff measurements.** Hydrogels with nanosensors were excited by a 785 nm laser with an incident power of 15 mW. Fluorescent images of hydrogels were collected with a 2D InGaAs detector (Princeton Instruments OMA V) paired with a Nikon AF Micro-Nikkor 60 mm f/2.8D lens and FEL 900 nm long-pass filter (Thorlabs). The typical integration time was 2 s.

**Hardware design.** The LED (LED670L, Thorlabs) was powered by 2V driving voltage. The typical current for nanosensor measurements was 45 mA. A photodetector (FGA21, Thorlabs) was biased at -3V with 1 MOhm load resistance, equipped with low-pass noise filter composed of 1 kOhm resistor and 0.1 μF capacitor. The power was delivered by a custom-made USB adapter connected to a personal computer. The optical power was measured by a power meter (Thorlabs). The electrical current was measured using Keithley 2002 and Labjack U7, and recorded using a custom-build LabVIEW software. A custom designed optical filters were used: 7 mm diameter 700 nm short-pass and 10 mm diameter 900 nm long-pass (Chroma). The enclosures to hold the electrical and optical components were custom designed in Solidworks and 3D printed in Ultimaker S3 using PLA material. System optimization was performed using translation stage manipulators (Thorlabs).

**Sensor performance measurements.** A hydrogel (10 mg/L nanotubes in 5x5x3 mm<sup>3</sup>) was placed into a miniaturized setup, if not stated otherwise. The nanosensor signal was calculated as the difference between photodetector current after and before the addition of the hydrogel. Noise values were calculated as a signal's standard deviation over 1000 sec time period, if not stated otherwise. The detector signal-to-noise ratio (SNR) was calculated as a ratio between nanosensor signal and noise levels. In this proof-of-concept study, it is important to note that all the measurements here were performed in-vitro.

**Analytical model.** The power emitted by LED was calculated using typical performance plots available in specs, alternatively it can also be measured experimentally. Spent power to drive LED was calculated as a product of driving voltage and current. To calculate light intensity on the hydrogel, we took into account LED spreading angle, distance to the hydrogel, and its area. Solid angles were approximated as referred to the central points of LED, hydrogel, and detector. LED emission was approximated as the one corresponding to the central LED wave-

length. Nanotube absorption in the hydrogel was calculated as a product of its absorbance, hydrogel thickness, and its concentration. The total nanotube emission was calculated using nanotube quantum yield of 1%. The emission wavelength was approximated as 1100 nm. We assume the emission is isotropic, i.e. emitted in 4π solid angle. Only a fraction of the emitted light will be detected by a photodetector, which will be determined by the distance to the detector and its area. The photocurrent was calculated as a product of the nanosensor emission that reached the detector and its responsivity. SNR was estimated as a ratio between the photocurrent and noise, which in turn was defined as a product of noise equivalent power and a square root of measurement bandwidth. The last two values were taken from the detector specs. To fit experimental data with the developed analytical model, a single correction factor of 12.5 was used to account for various limitation of the model, such as reflections at interfaces, single emission and fluorescence wavelength, and solid angle approximations.

## RESULTS AND DISCUSSION

**Nanosensor Characterization** The progesterone Corona Phase Molecular Recognition (CoPhMoRe) sensor was prepared by suspending SWCNT synthesized by the high-pressure carbon monoxide (HiPCO) process with specifically designed templated polymers (SM8).<sup>45</sup> Successful SWCNT dispersion with polymer was confirmed via UV-Vis-nIR spectroscopy, which revealed sharp, distinct absorption peaks characteristic of isolated SWCNT (Fig. 2a). Near-infrared (nIR) emission spectra of the dispersion, both before and after the addition of 100 μM progesterone, were captured under 785 nm laser excitation (Fig. 2b).<sup>45</sup> The sensor demonstrated a significant turn-on response, exhibiting a 58% increase in fluorescence, measured by integrating the total emission intensity across the spectrum, compared to a 23% response (magnitude) for the second highest steroid response at the same concentration of 100 μM.

The SWCNT sensor was encapsulated in a biocompatible hydrogel (Fig. 2d-e) matrix for *in vivo* application. Peak position and relative peak intensity of SM8-SWCNT in both absorption and fluorescence emission spectra remained consistent (Fig. 2c, Fig. S1), indicating nearly identical dielectric environments surrounding the SWCNT in solution and hydrogel form. The sensor's functionality within the hydrogel was confirmed through its response to progesterone at a concentration of 100 μM dispersed in phosphate buffer saline (PBS)-2% dimethylsulfoxide (DMSO) buffer, with control measurements in buffer showing no intensity changes (Fig. 2f). The sensor's response across both solution and hydrogel phases to varying progesterone concentrations was quantitatively analyzed using the following functional form:

$$\frac{I - I_0}{I_0} = \beta \frac{C}{C + K_d} \quad (\text{Eq.1})$$

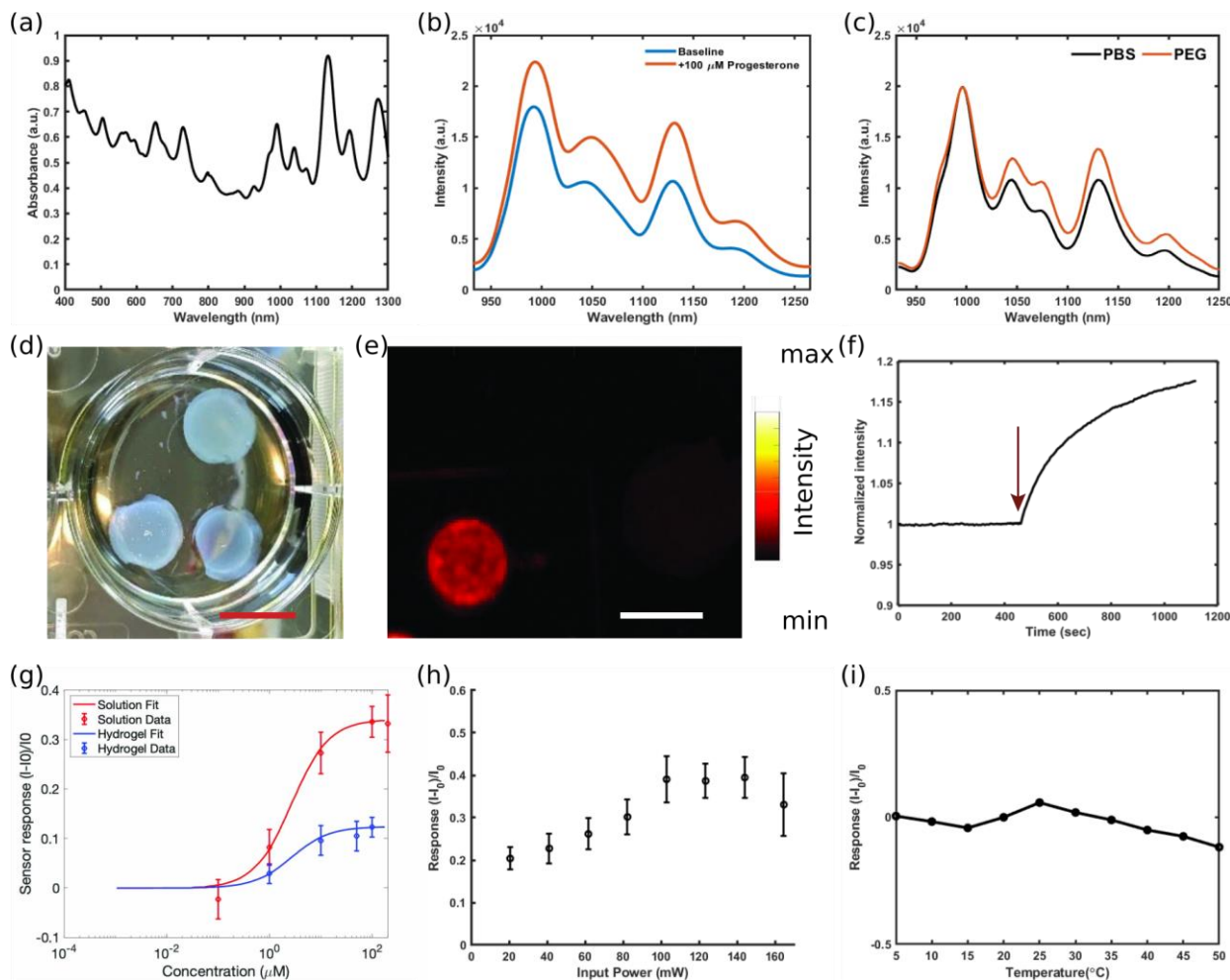


**Figure 2.** Nanosensor characterization. (a) UV-Vis-nIR absorption spectrum of polymer-SWCNT dispersion (6.8 mg/L). (b) Fluorescence emission spectra of the nanosensor (1 mg/L) before and after the addition of 100  $\mu$ M progesterone hormone.<sup>45</sup> Reprinted from Lee et al, *Advanced Healthcare Materials*, 9, 2020, with permission from Wiley-VCH. (c) Fluorescence spectra of the progesterone sensor in buffer condition and in PEGDA hydrogel solution before crosslinking. (d) Visible images of PEGDA-8000 hydrogels encapsulated with nanosensors (10 mg/L). Scale bars are 5 mm. (e) A near-infrared fluorescent image of the hydrogel nanosensor (10 mg/L). Scale bars are 5 mm. (f) Normalized fluorescent intensity of a hydrogel nanosensor (10 mg/L) in a buffer solution with the addition of progesterone (final conc: 100  $\mu$ M) at  $t = 450$  sec. (g) Calibration curves and the analytical model fits for nanosensors in solution and in the hydrogel (data presented as mean  $\pm$  SEM,  $n = 3$ ). (h) Nanosensor response towards 100  $\mu$ M progesterone as a function of illumination power in solution and in the hydrogel (data presented as mean  $\pm$  SEM,  $n = 3$ ). (i) Normalized photoluminescence intensity changes as a function of the nanosensor solution temperature (data presented as mean  $\pm$  SEM,  $n = 3$ ).

where  $I$  is the fluorescence intensity after progesterone addition,  $I_0$  is the original intensity,  $\beta$  is the proportionality factor between analyte occupancy and fluorescence intensity change,  $C$  is the progesterone concentration, and  $K_D$  is the equilibrium dissociation constant (**Fig. 2g**). The SWCNT sensor was responsive to progesterone from 1  $\mu$ M to 200  $\mu$ M, serving as a robust quantitative tool to study the progesterone concentration in marine animals. The hydrogel-phase SWCNT exhibited a lower magnitude of response to progesterone when compared to the solution phase counterpart, likely associated to the constraints of the SWCNT-polymer movements inside the cross-linked hydrogel matrix.

It is important to note that the sensors developed here are based on our previous study<sup>42</sup>, where specificity of the sensor's response towards progesterone against other in-

terfering hormones were thoroughly investigated. Additionally, the stability of and reversibility of response of sensors encapsulated in hydrogel response were also discussed.

The sensor response demonstrated a dependency on illumination power (**Fig. 2h**), with optimal performance observed at approximately 100 mW. This finding suggests the potential of preserving the sensor functionality while reducing the power requirement for the miniaturized tag. As the sensor would be ultimately deployed in marine environment with varied weather conditions, we investigated the sensor fluorescence at different temperature (**Fig. 2i**). The normalized SWCNT fluorescence was relatively stable from 5  $^{\circ}$ C to 35  $^{\circ}$ C, and started to decrease at higher temperatures. The observed stability further supports the hypothesis that sensor response stability can be



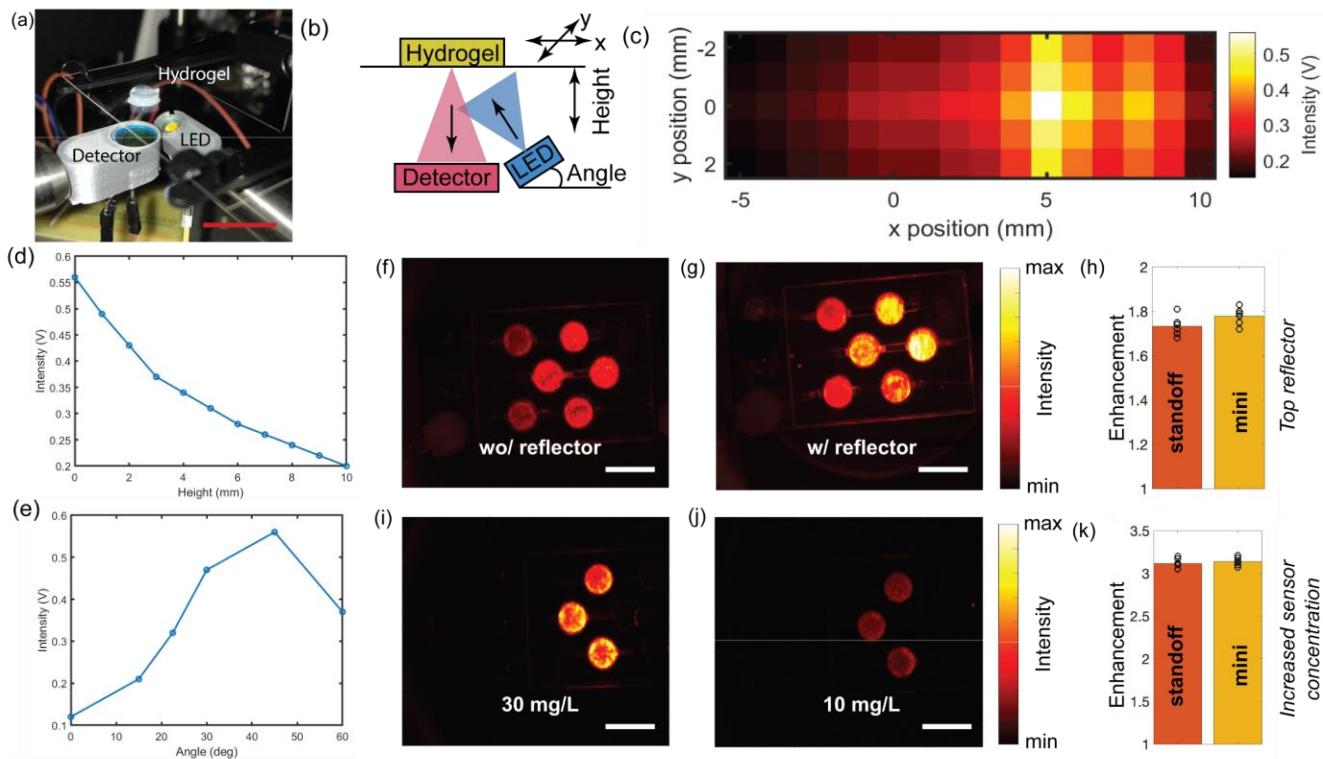


**Figure 3.** Hardware optimization with a 3D-printed modular setup. (a) An experimental modular setup with LED and its short-pass optical filter, a photodetector and its long-pass optical filter, and a glass slide supporting nanosensor hydrogel (10 mg/L nanotubes in  $5 \times 3 \times 3$  mm<sup>3</sup>). Exact positions of the components are controlled by precise micromanipulators. Scale bar is 1 cm. (b) Schematic illustration of the experimental system in (a). (c) Nanosensor fluorescence as a function of the relative component positions. The center of the detector is located at (0,0), while the center of LED is at (10,0) with an inclination angle of 45°. (d) Nanosensor fluorescence decreases with the hydrogel height above the electronic components. (e) Nanosensor fluorescence as a function of the LED inclination angle. (f,g) A near-infrared image of six nanosensor hydrogels without (f) and with (g) a top reflector made out of silver mirror. Scale bars are 1 cm. (h) Top reflector enhancement for standoff (red) and mini (yellow) setups. (i,j) A near-infrared image of three hydrogels with 30 mg/L (i) and 10 mg/L (j) nanosensors. (k) Fluorescence signal enhancements for standoff (red) and mini (yellow) setups for increased sensor concentrations.

enhanced through encapsulation in hydrogels. Hydrogels exhibit greater stability at lower temperatures compared to higher temperatures, as lower temperatures mitigate water molecule loss and prevent dehydration. The observed changes in fluorescence intensity at elevated temperatures may be attributed to the rearrangement of the corona phase on the surface of the carbon nanotube. The raw fluorescence spectra at each temperature are presented in Fig. S2. The temperature range examined in this study should be sufficient, as the temperature in marine environments varies between 0°C and 30°C, depending on factors such as water depth, geographic location (e.g., proximity to the equator or polar regions), and the time of year.

**Engineering Design for Miniaturized Fluorescent Tag** A central goal of this work is to integrate the hydrogel sensor with existing acoustic fish tags, ones designed to conform to movement of marine animals. As such, the miniaturization into and attachment methods of a flexible form factor are critical next steps. We have encapsulated the developed nanosensors into a compact fluorescent tag, incorporating integrated excitation and detection optical paths. To optimize the tag's optoelectronic performance, we selected several commercially available

components. For the photodetection, we evaluated InGaAs photodiodes, specifically Thorlabs' FGA21, FGA10, and FDGA05 (Table S1) models, which vary in active area and noise levels. Ultimately, the FGA21 was chosen for benchmarking. For excitation, we chose Thorlabs' LEDs - LED630L, LED645L, and LED670L (Table S2) - that emit light at varying wavelengths. Given the minimal variations in nanosensor absorption in this part of the spectrum and the lower power demand, we have chosen to work with the LED670L. The performance of other photodetectors and LEDs can be estimated with a simple scaling analysis using an analytical model discussed below. See **Experimental Section** for the details on electrical circuit.

To find an optimal hardware design of the tag, we have 3D-printed a modular setup, where positions of an LED with the supporting 700 nm short-pass optical filter and the photodetector with the supporting 900 nm long-pass optical filter were controlled by micromanipulators (Fig. 3a). The nanosensor hydrogel was placed on a glass cover slip above the hardware, configured in an inverted fluorescent setup where the LED was fixed in a slanted position to prevent direct reflection into the photodetector (Fig. 3b). This configuration facilitated extensive optimi

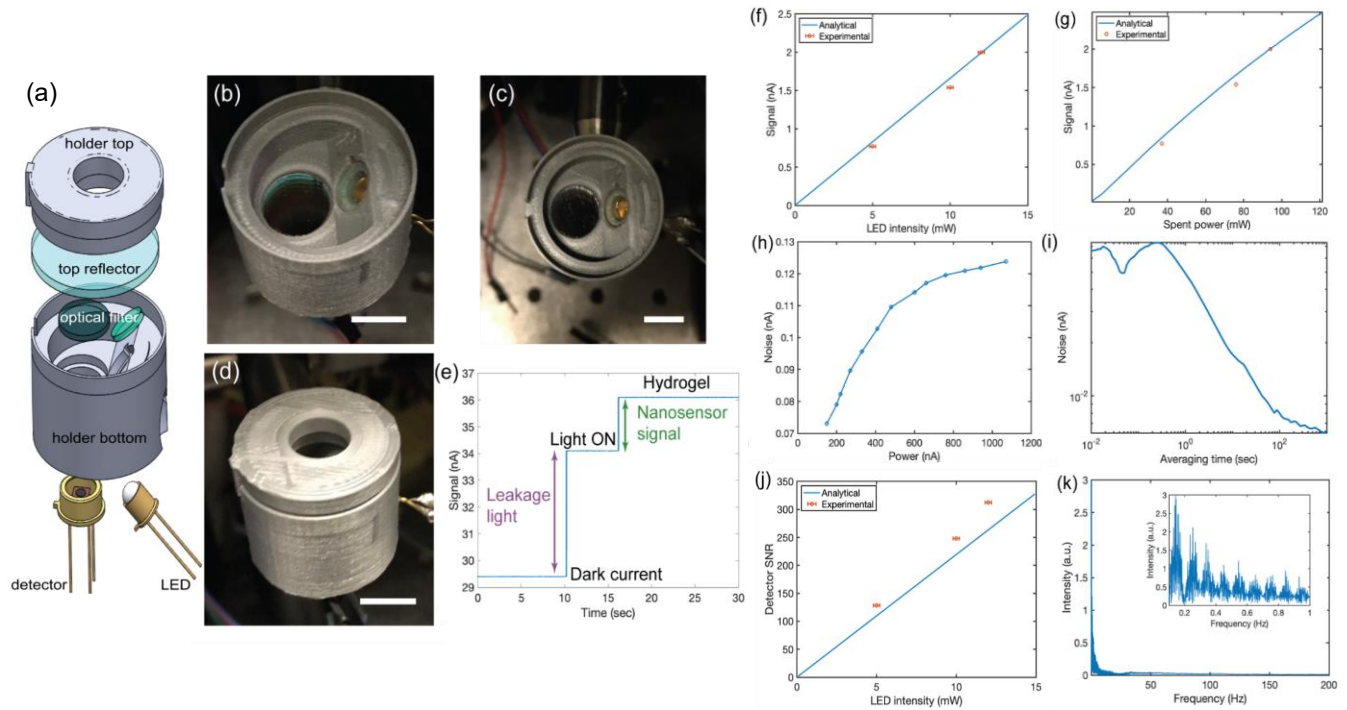


**Figure 4.** System performance. (a-d) A schematic overview (a) and photographs (b-d) of the miniaturized fluorescence setup. Scale bars are 1 cm. (e) Photodetector current in response to the hydrogel (10 mg/L nanotubes in  $5 \times 5 \times 3$  mm<sup>3</sup>). (f) Experimental measurements and analytical model for photodetector current detected from the hydrogel in response to various excitation LED powers. (g) Same as (f), but for spent electrical power used to drive LED. (h) The measured noise of the photodetector as a function of the total power. (i) The photodetector noise for 50 nA total photocurrent averaged over various times. (j) Experimental measurements and analytical model for the photodetector SNR as in (g) with an averaging time of 1000 sec. (k) FFT spectrum of the photodetector signal with low-frequency components shown in the inset.

zation studies, adjusting geometrical parameters to enhance performance. In particular, optimal position of the hydrogel with respect to the LED and the photodetector was found (Fig. 3c), noting that increasing the distance between the hydrogel and electronics reduced the detected signal (Fig. 3d). Additionally, an LED inclination of 45° was found to be optimal for maximizing detection efficiency (Fig. 3e).

To enhance the signal further, the setup can be modified to include a top reflector. Introducing a silver mirror above the hydrogels (Fig. 3f, g) extends the excitation path, increasing the fluorescent signal by 70% as evidenced in both the standard standoff and miniaturized setups (Fig. 3h). To accommodate such an arrangement, a capping system from Figure 1 may be modified to include access channels for sensing species to reach nanosensors. Additionally, the nanosensor concentration can be increased up to 30 mg/L from the standard 10 mg/L that we kept in this work, which also increases its fluorescent signal by 3.1 times (Fig. 3i-k). However, further concentration increases can lead to incompatibility between the nanosensor and the hydrogel matrix, along with enhanced light reabsorption, limiting its fluorescence output.

Using the optimized configuration, we have prototyped a miniaturized fluorescent tag using 3D printed mold that houses electronic and optical components, as well as the nanosensor hydrogel (Fig. 4a-d). The assembly process in-

volves inserting electronic components from the back, placing optical filters and a cover slip glass from above, and securing the hydrogel with a top holder. For accurate nanosensor measurements, it's critical to distinguish the nanosensor signal from the dark current and leakage light current (Fig. 4e). The presence of the incident light leakage is associated with the fact that the interferometric filters used in our case deviate from their optimal performance in the presence of angled incidence light caused by the system miniaturization. As such the sensor signal is calculated by subtracting both the dark current and the leakage light measured in the absence of the hydrogel from the total signal measured in the presence of the hydrogel. Typically, with several milliwatts of optical power emitted by LED, we detect several nanoamperes of photocurrent emitted by the hydrogel nanosensor (Fig. 4f, g). Our analytical model detailed in the **Experimental** section, demonstrates excellent agreement with the experimental measurements, providing a powerful prediction tool to rapidly evaluate and optimize various system parameters.

We further assessed noise levels of the photodetector, defining it as the signal's standard deviation. We found that the dark current noise represents a dominant component, while the shot noise plays a minor role, increasing slowly with the photocurrent (Fig. 4h). The noise levels decrease over 10x when the signal is averaged over extended periods of time (Fig. 4i). Overall, the miniaturized setup demonstrates signal-to-noise ratio (SNR) values over 300 for the hydrogel nanosensors (Fig. 4j),

providing the ability to track nanosensor response in real-time. The Fast Fourier Transform (FFT) analysis of the signal does not reveal any dominant peaks and largely follows  $1/f$ -noise pattern (Fig. 4k).

**Nanosensor Performance in the Optimized Hardware** Encouraged by high SNR values of the miniaturized setup, we further tested the ability to detect the nanosensor response to the progesterone hormone in the mini setup. Sensor performance was assessed by measuring its fluorescent intensity before and 1000 s after hormone addition, allowing the sensor signal to stabilize. Due to its binding mechanism, the response of this type of sensor is measured as a normalized intensity change. The developed miniaturized setup successfully detected the addition of 100  $\mu\text{M}$  of progesterone, with a  $\sim 15\%$  turn-on response (Fig. 5a). In contrast, control measurements with buffer showed no sensor changes (Fig. 5b). The miniaturized setup also showed different degrees of the nanosensor fluorescence increase in response to different progesterone concentrations (Fig. 5a). These results are detailed in the calibration curve that fits the data to a sigmoidal model of nanosensor binding (Fig. 5c), which shows excellent reproducibility and repeatability. The limit of detection (LOD) for the miniaturized setup was determined as 100 nM. This value was calculated by adding the intensity change of the nanosensor from the addition of only buffer (Sblank) and three times the standard deviation ( $\sigma_{\text{blank}}$ ) of the response as the noise level. Additionally, the nanosensor was exposed to alternating cycles of 0 and 100  $\mu\text{M}$  progesterone in 1X PBS with 2% DMSO (Fig. 5d). The sensor hydrogel exhibited a stable and reversible response, allowing perturbations in fluorescence – an important feature for continuous measurements.

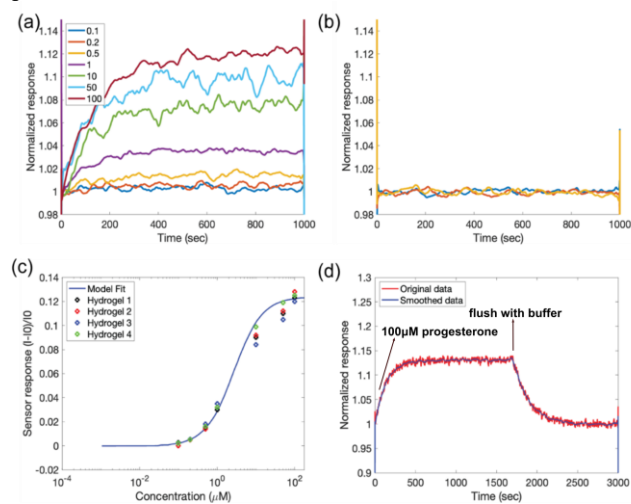


**Figure 5.** Nanosensor sensing performance in mimic condition. (a) Normalized response of the hydrogel nanosensor (10 mg/L nanotubes in  $5 \times 5 \times 3 \text{ mm}^3$ ) as measured in the miniaturized setup to various progesterone concentration introduced at  $t = 0$ , given in micromolars. (b) Representative control measurements. (c) Calibration curve of the hydrogel nanosensor response. (d) Normalized response of the hydrogel nanosensor for reversibility studies, where 100  $\mu\text{M}$  progester-

one was introduced at  $t = 0$  and the system was flushed with buffer after  $t = 1800 \text{ sec}$ .

**Performance Metrics for Miniaturized Fluorescent Tags** Sensor SNR and power consumption are two important metrics for field deployment of fluorescent tags. Noise, particularly normalized against signal strength, is the principal limiting factor for measurement accuracy. The normalized noise level determines the ability to detect fluorescent changes and can be related to the limit of detection using the experimentally determined calibration curve. Taking the limit of detection as 3x noise level and assessing noise levels measured in various experiments (Fig. 6a), we find a tradeoff between those quantities. Noise levels change slightly from measurement to measurements, probably due to hydrogel variations and mechanical instabilities. Our results indicate that we can successfully detect down to 100 nM of progesterone.

To understand the energy budget to operate such a sensor in-field, we calculated the expected battery life for a standard 2000 mAh battery under different usage frequencies (Fig. 6b). Depending on the measurement frequency that can range from once in 10 days to 10 times per day, the battery can last from 2000 days to 10 days, respectively. Importantly, we note that reducing the average measurement duration from 1000 sec to 100 sec increases noise by only 20%, suggesting a potential for extending battery life with minimal impact on data quality. The range of progesterone levels across a wide variety of marine organisms is between 0.32 nM and 300 nM,<sup>33–35,47–51</sup> and these levels can fluctuate over periods ranging from minutes to months. The sensitivity of our sensor system overlaps with a substantial portion of this range. For example, Gesto et al.<sup>50</sup> measured cortisol levels in rainbow trout and zebra fish, finding that the latter expressed 47.5 nM in the control group but 298 nM in the stressed cohort. The former value is below the detection limit demonstrated in this work by a factor of 2 but the latter case, of significant interest, is above by a factor of 3. Similarly, Nouri et al.<sup>51</sup> measured steroid hormones in Large-mouth bass, LMB (*Micropterus salmoides*), fathead minnow, FHM (*Pimephales promelas*), zebrafish (*Danio rerio*) and silverside (*Menidia beryllina*) using an LC-MS/MS technique with a 38.2 pM instrument detection limit. They measured a hormone concentration of 287.8 nM for the average of the four species. The sensor system demonstrated in this work may also find use in studies examining the uptake of hormone additives to fish farm production. Khatun et al.<sup>52</sup> studied testosterone, estrogen and progesterone addition to rui (*Labeo rohita*), catla (*Catla catla*), and monosex tilapia (*Oreochromis niloticus*), and found that progesterone levels in all three fish types ranged from 100 nM to 2326 nM. Our device requires further refinement to accurately monitor these variations with precise spatial and temporal resolution. For extended studies, it will be critical to enhance the nanosensors' stability, improve reference corrections, and implement measures to prevent biofouling.



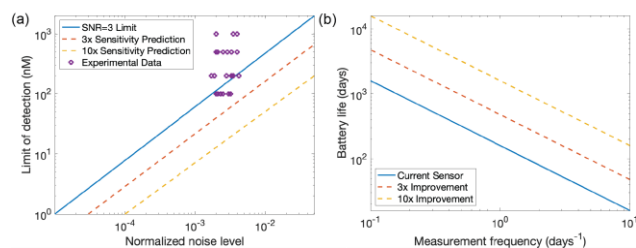


**Figure 6.** Performance metrics. (a) Limit of detection dependence of the normalized noise limit with SNR=3 line extracted from the calibration curve in Fig. 4. (b) A tradeoff between battery life and measurement frequency for 2000 mAh battery averaging a signal over 1000 sec for one measurement.

## CONCLUSIONS AND FUTURE WORK

In this study, we engineered a miniaturized, implantable fluorescent tag designed for continuous monitoring of progesterone in marine animals, integrating a CoPh-MoRe-based nanosensor within a biocompatible hydrogel matrix. This tag, optimized to conform to marine animal dynamics, provides selective and reversible responses to progesterone across physiologically relevant concentrations. Systematic characterization under various environmental conditions confirmed the tag's robustness, with a detection limit of 100 nM and a dynamic range extending to 200  $\mu$ M. Our integrated sensing platform demonstrated exceptional optoelectronic customization for minimized power consumption and enhanced signal-to-noise ratio, proving suitable for long-term hormone monitoring and deployment in marine environments. The application of an analytical model enables predictive assessments of performance, guiding further device optimization.

This work represents the first demonstration of a SWCNT nanosensor-enabled implantable platform for continuous *in vivo* hormone monitoring in marine animals. The ability to track hormone levels with high spatiotemporal resolution will open up new avenues for studying the complex interplay between animal physiology, behavior, and their environment. The fundamental advances in sensor design and performance realized here are applicable to a wide range of analytes and ocean sensing scenarios.

Future work will focus on further miniaturization and packaging of the tag for field deployment, enabled by the rapidly expanding toolbox of flexible electronics, wireless power transfer, and embedded data processing. Incorporating multi-modal sensing capabilities and orthogonal sensors will enhance the information yield per animal and provide a more holistic view of marine ecosystem dynamics. We anticipate that this new sensing paradigm will greatly complement and expand the capabilities of conventional marine biologging, enabling smarter and more agile marine conservation and resource management.

## ASSOCIATED CONTENT

**Supporting Information.** UV-Vis absorption spectrum of the progesterone sensor in buffer condition and in hydrogel

solution before crosslinking, raw fluorescence emission spectra of the nanosensor at different solution temperature, specifications of photodiode, specifications of LEDs. The Supporting Information is available free of charge on the ACS Publication website.

## AUTHOR INFORMATION

Corresponding Author

\* Email: strano@mit.edu

## Author Contributions

The manuscript was written through contributions of all authors. All authors have given approval to the final version of the manuscript.

## Notes

The authors declare no competing financial interests.

## ACKNOWLEDGMENT

This work was supported by the Innovasea System Inc (Agrmt dated 02/04/2021). X.J. acknowledges support from Mathworks Inc. through the Mathworks Engineering Fellowship. The authors also acknowledge support from the National Science Foundation (Award no. CBET-2124194) for nanoparticle spectroscopy and characterization. The collaborative discussions on the biologging problem were supported by King Abdullah University of Science & Technology (OSR-2015 Sensors 2707). The Table of Contents (ToC) figure was created with Biorender.com.

## ABBREVIATIONS

SWCNT, single walled carbon nanotube; PEGDA, poly (ethylene glycol) diacrylate; GPS, global positioning system; GSD, genotypic sex determination; TSD, temperature-dependent sex determination; near-infrared (nIR); LED, light-emitting diode; HiPCO, High-Pressure Carbon Monoxide; TEA, trimethylamine; THF, tetrahydrofuran; HCl, hydrogen chloride; DCM, dichloromethane; MEHQ, Hydroquinone monomethyl ether; InGaAs, indium gallium arsenide; SNR, signal-to-noise ratio; CoPhMore, corona phase molecular recognition; DMSO, dimethylsulfoxide; PBS, phosphate buffer saline; FFT, fast fourier transform analysis;

## REFERENCES

- (1) Kaidarova, A.; Geraldi, N. R.; Wilson, R. P.; Kosel, J.; Meekan, M. G.; Eguíluz, V. M.; Hussain, M. M.; Shamim, A.; Liao, H.; Srivastava, M.; Saha, S. S.; Strano, M. S.; Zhang, X.; Ooi, B. S.; Holton, M.; Hopkins, L. W.; Jin, X.; Gong, X.; Quintana, F.; Tovasarov, A.; Tasmagambetova, A.; Duarte, C. M. Wearable Sensors for Monitoring Marine Environments and Their Inhabitants. *Nature Biotechnology* **2023**, *41* (9), 1208–1220. <https://doi.org/10.1038/s41587-023-01827-3>.
- (2) Chung, H.; Lee, J.; Lee, W. Y. A Review: Marine Biologging of Animal Behaviour and Ocean Environments. *Ocean Science Journal* **2021**, *56* (2), 117–131. <https://doi.org/10.1007/s12601-021-00015-1>.
- (3) Hussey, N. E.; Kessel, S. T.; Aarestrup, K.; Cooke, S. J.; Cowley, P. D.; Fisk, A. T.; Harcourt, R. G.; Holland, K. N.; Iverson, S. J.; Kocik, J. F.; Flemming, J. E. M.; Whoriskey, F. G. Aquatic Animal Telemetry: A Panoramic Window into the Underwater World. *Science* **2015**, *348* (6240),

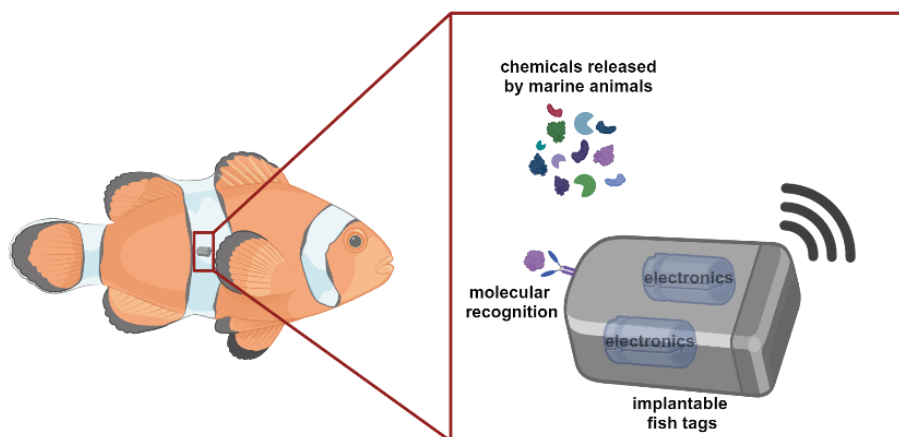
- (4) Harcourt, R.; Sequeira, A. M. M.; Zhang, X.; Roquet, F.; Komatsu, K.; Heupel, M.; McMahon, C.; Whoriskey, F.; Meekan, M.; Carroll, G.; Brodie, S.; Simpfendorfer, C.; Hindell, M.; Jonsen, I.; Costa, D. P.; Block, B.; Muelbert, M.; Woodward, B.; Weise, M.; Aarestrup, K.; Biuw, M.; Boehme, L.; Bograd, S. J.; Cazau, D.; Charrassin, J. B.; Cooke, S. J.; Cowley, P.; de Bruyn, P. J. N.; Jeanniard du Dot, T.; Duarte, C.; Eguíluz, V. M.; Ferreira, L. C.; Fernández-Gracia, J.; Goetz, K.; Goto, Y.; Guinet, C.; Hammill, M.; Hays, G. C.; Hazen, E. L.; Hückstädt, L. A.; Huvener, C.; Iverson, S.; Jaaman, S. A.; Kittiwattana, K.; Kovacs, K. M.; Lydersen, C.; Moltmann, T.; Naruoka, M.; Phillips, L.; Picard, B.; Queiroz, N.; Reverdin, G.; Sato, K.; Sims, D. W.; Thorstad, E. B.; Thums, M.; Treasure, A. M.; Trites, A. W.; Williams, G. D.; Yonehara, Y.; Fedak, M. A. Animal-Borne Telemetry: An Integral Component of the Ocean Observing Toolkit. *Frontiers in Marine Science* **2019**, *6* (JUN), 436861. <https://doi.org/10.3389/FMARS.2019.00326/BIBTEX>.
- (5) Watanabe, Y. Y.; Papastamatiou, Y. P. Biologging and Biotelemetry: Tools for Understanding the Lives and Environments of Marine Animals. *Annual Review of Animal Biosciences* **2023**, *11* (Volume 11, 2023), 247–267. <https://doi.org/10.1146/ANNUREV-ANIMAL-050322-073657/CITE/REFWORKS>.
- (6) Roquet, F.; Boehme, L.; Fedak, M.; Block, B.; Charrassin, J.-B.; Costa, D.; Hückstädt, L.; Guinet, C.; Harcourt, R.; Hindell, M.; McMahon, C.; Woodward, B. Ocean Observations Using Tagged Animals. *Oceanography* **2017**, *30* (2), 139–139. <https://doi.org/10.5670/OCEANOGRAPHY.2017.235>.
- (7) Hays, G. C.; Bailey, H.; Bograd, S. J.; Bowen, W. D.; Campagna, C.; Carmichael, R. H.; Casale, P.; Chiaradia, A.; Costa, D. P.; Cuevas, E.; Nico de Bruyn, P. J.; Dias, M. P.; Duarte, C. M.; Dunn, D. C.; Dutton, P. H.; Esteban, N.; Friedlaender, A.; Goetz, K. T.; Godley, B. J.; Halpin, P. N.; Hamann, M.; Hammerschlag, N.; Harcourt, R.; Harrison, A. L.; Hazen, E. L.; Heupel, M. R.; Hoyt, E.; Humphries, N. E.; Kot, C. Y.; Lea, J. S. E.; Marsh, H.; Maxwell, S. M.; McMahon, C. R.; Notarbartolo di Sciara, G.; Palacios, D. M.; Phillips, R. A.; Righton, D.; Schofield, G.; Seminoff, J. A.; Simpfendorfer, C. A.; Sims, D. W.; Takahashi, A.; Tetley, M. J.; Thums, M.; Trathan, P. N.; Villegas-Amtmann, S.; Wells, R. S.; Whiting, S. D.; Wildermann, N. E.; Sequeira, A. M. M. Translating Marine Animal Tracking Data into Conservation Policy and Management. *Trends in ecology & evolution* **2019**, *34* (5), 459–473. <https://doi.org/10.1016/J.TREE.2019.01.009>.
- (8) Wilson, R. P.; Gómez-Laich, A.; Sala, J. E.; Dell'Omo, G.; Holton, M. D.; Quintana, F. Long Necks Enhance and Constrain Foraging Capacity in Aquatic Vertebrates. *Proceedings of the Royal Society B: Biological Sciences* **2017**, *284* (1867). <https://doi.org/10.1098/RSPB.2017.2072>.
- (9) Hindell, M. A.; Reisinger, R. R.; Ropert-Coudert, Y.; Hückstädt, L. A.; Trathan, P. N.; Bornemann, H.; Charrassin, J. B.; Chown, S. L.; Costa, D. P.; Danis, B.; Lea, M. A.; Thompson, D.; Torres, L. G.; Van de Putte, A. P.; Alderman, R.; Andrews-Goff, V.; Arthur, B.; Ballard, G.; Bengtson, J.; Bester, M. N.; Blix, A. S.; Boehme, L.; Bost, C. A.; Boveng, P.; Clelland, J.; Constantine, R.; Corney, S.; Crawford, R. J. M.; Dalla Rosa, L.; de Bruyn, P. J. N.; Delord, K.; Descamps, S.; Double, M.; Emmerson, L.; Fedak, M.; Friedlaender, A.; Gales, N.; Goebel, M. E.; Goetz, K. T.; Guinet, C.; Goldsworthy, S. D.; Harcourt, R.; Hinke, J. T.; Jerosch, K.; Kato, A.; Kerry, K. R.; Kirkwood, R.; Kooyman, G. L.; Kovacs, K. M.; Lawton, K.; Lowther, A. D.; Lydersen, C.; Lyver, P. O. B.; Makhado, A. B.; Márquez, M. E. I.; McDonald, B. I.; McMahon, C. R.; Muelbert, M.; Nachtsheim, D.; Nicholls, K. W.; Nordøy, E. S.; Olmastroni, S.; Phillips, R. A.; Pistorius, P.; Plötz, J.; Pütz, K.; Ratcliffe, N.; Ryan, P. G.; Santos, M.; Southwell, C.; Staniland, I.; Takahashi, A.; Tarroux, A.; Trivelpiece, W.; Wakefield, E.; Weimerskirch, H.; Wienecke, B.; Xavier, J. C.; Wotherspoon, S.; Jonsen, I. D.; Raymond, B. Tracking of Marine Predators to Protect Southern Ocean Ecosystems. *Nature* **2020**, *580*:7801, 2020, 580 (7801), 87–92. <https://doi.org/10.1038/s41586-020-2126-y>.
- (10) Barrionuevo, M.; Ciancio, J.; Steinfurth, A.; Frere, E. Geolocation and Stable Isotopes Indicate Habitat Segregation between Sexes in Magellanic Penguins during the Winter Dispersion. *Journal of Avian Biology* **2020**, *51* (2). <https://doi.org/10.1111/JAV.02325>.
- (11) Wilmers, C. C.; Nickel, B.; Bryce, C. M.; Smith, J. A.; Wheat, R. E.; Yovovich, V. The Golden Age of Bio-logging: How Animal-borne Sensors Are Advancing the Frontiers of Ecology. *Ecology* **2015**, *96* (7), 1741–1753. <https://doi.org/10.1890/14-1401.1>.
- (12) Block, B. A.; Jonsen, I. D.; Jorgensen, S. J.; Winship, A. J.; Shaffer, S. A.; Bograd, S. J.; Hazen, E. L.; Foley, D. G.; Breed, G. A.; Harrison, A. L.; Ganong, J. E.; Swithenbank, A.; Castleton, M.; Dewar, H.; Mate, B. R.; Shillinger, G. L.; Schaefer, K. M.; Benson, S. R.; Weise, M. J.; Henry, R. W.; Costa, D. P. Tracking Apex Marine Predator Movements in a Dynamic Ocean. *Nature* **2011**, *475* (7354), 86–90. <https://doi.org/10.1038/nature10082>.
- (13) Watanabe, Y. Y.; Goldbogen, J. A. Too Big to Study? The Biologging Approach to Understanding the Behavioural Energetics of Ocean Giants. *Journal of Experimental Biology* **2021**, *224* (13). <https://doi.org/10.1242/jeb.202747>.
- (14) Jorgensen, S. J.; Reeb, C. A.; Chapple, T. K.; Anderson, S.; Perle, C.; Van Sommeran, S. R.; Fritz-Cope, C.; Brown, A. C.; Klimley, A. P.; Block, B. A. Philopatry and Migration of Pacific White Sharks. *Proceedings of the Royal Society B: Biological Sciences* **2010**, *277* (1682), 679. <https://doi.org/10.1098/RSPB.2009.1155>.
- (15) Gleiss, A. C.; Jorgensen, S. J.; Liebsch, N.; Sala, J. E.; Norman, B.; Hays, G. C.; Quintana, F.; Grundy, E.; Campagna, C.; Trites, A. W.; Block, B. A.; Wilson, R. P. Convergent Evolution in Locomotory Patterns of Flying and Swimming Animals. *Nature Communications* **2011**, *2* (1), 1–7. <https://doi.org/10.1038/ncomms1350>.
- (16) Cooke, S. J.; Hinch, S. G.; Wikelski, M.; Andrews, R. D.; Kuchel, L. J.; Wolcott, T. G.; Butler, P. J. Biotelemetry: A Mechanistic Approach to Ecology. *Trends in Ecology & Evolution* **2004**, *19* (6), 334–343. <https://doi.org/10.1016/J.TREE.2004.04.003>.
- (17) Meekan, M. G.; Fuiman, L. A.; Davis, R.; Berger, Y.; Thums, M. Swimming Strategy and Body Plan of the World's Largest Fish: Implications for Foraging Efficiency and Thermoregulation. *Frontiers in Marine Science* **2015**, *2* (SEP). <https://doi.org/10.3389/FMARS.2015.00064>.
- (18) Ripberger, S. P.; Carter, G. G.; Page Supervision, R. A.; Duda, N.; Koelpin, A.; Weigel, R.; Hartmann, M.; Nowak, T.; Thielecke, J.; Schadhauser, M.; Robert, J.; Herbst, S.; Meyer-Wegener, K.; Wägemann, P.; Preikschat, W. S.; Cassens, B.; Kapitza, R.; Dressler, F.; Mayer, F. Thinking Small: Next-Generation Sensor Networks Close the Size Gap in Vertebrate Biologging. *PLoS Biology* **2020**, *18* (4), 1–25. <https://doi.org/10.1371/journal.pbio.3000655>.
- (19) Delord, K.; Barbraud, C.; Pinaud, D.; Letournel, B.; Jaugeon, B.; Goraguer, H.; Lazure, P.; Lormée, H. Movements of Three Alcid Species Breeding Sympatrically in

- Saint Pierre and Miquelon, Northwestern Atlantic Ocean. *Journal of Ornithology* **2020**, *161* (2), 359–371. <https://doi.org/10.1007/S10336-019-01725-Z/FIGURES/4>.
- (20) Ware, C.; Trites, A. W.; Rosen, D. A. S.; Potvin, J. Averaged Propulsive Body Acceleration (APBA) Can Be Calculated from Biologging Tags That Incorporate Gyroscopes and Accelerometers to Estimate Swimming Speed, Hydrodynamic Drag and Energy Expenditure for Steller Sea Lions. *PLOS ONE* **2016**, *11* (6), e0157326. <https://doi.org/10.1371/JOURNAL.PONE.0157326>.
  - (21) Nassar, J. M.; Khan, S. M.; Velling, S. J.; Diaz-Gaxiola, A.; Shaikh, S. F.; Gerdali, N. R.; Torres Sevilla, G. A.; Duarte, C. M.; Hussain, M. M. Compliant Lightweight Non-Invasive Standalone “Marine Skin” Tagging System. *npj Flexible Electronics* **2018**, *2* (1), 1–9. <https://doi.org/10.1038/s41528-018-0025-1>.
  - (22) Lee, M. A.; Duarte, C. M.; Eguiluz, V. M.; Heller, D. A.; Langer, R.; Meekan, M. G.; Sikes, H. D.; Srivastava, M.; Strano, M. S.; Wilson, R. P. Can Fish and Cell Phones Teach Us about Our Health? *ACS Sensors* **2019**, *4* (10), 2566–2570. <https://doi.org/10.1021/acssensors.9b00947>.
  - (23) Kaidarova, A.; Gerdali, N. R.; Wilson, R. P.; Kosel, J.; Meekan, M. G.; Eguiluz, V. M.; Hussain, M. M.; Shamim, A.; Liao, H.; Srivastava, M.; Saha, S. S.; Strano, M. S.; Zhang, X.; Ooi, B. S.; Holton, M.; Hopkins, L. W.; Jin, X.; Gong, X.; Quintana, F.; Tovasarov, A.; Tasmagambetova, A.; Duarte, C. M. Wearable Sensors for Monitoring Marine Environments and Their Inhabitants. *Nature Biotechnology* **2023**, *41* (9), 1208–1220. <https://doi.org/10.1038/s41587-023-01827-3>.
  - (24) Cooke, S. J.; Brownscombe, J. W.; Raby, G. D.; Broell, F.; Hinch, S. G.; Clark, T. D.; Semmens, J. M. Remote Bioenergetics Measurements in Wild Fish: Opportunities and Challenges. *Comparative Biochemistry and Physiology - Part A: Molecular and Integrative Physiology* **2016**, *202*, 23–37. <https://doi.org/10.1016/j.cbpa.2016.03.022>.
  - (25) Madliger, C. L.; Love, O. P.; Hultine, K. R.; Cooke, S. J. The Conservation Physiology Toolbox: Status and Opportunities. *Conservation Physiology* **2018**, *6* (1), 29. <https://doi.org/10.1093/CONPHYS/COY029>.
  - (26) Ojogoro, J. O.; Scrimshaw, M. D.; Sumpter, J. P. Steroid Hormones in the Aquatic Environment. *The Science of the total environment* **2021**, 792. <https://doi.org/10.1016/J.SCITOTENV.2021.148306>.
  - (27) Azizi-Lalabadi, M.; Pirsahab, M. Investigation of Steroid Hormone Residues in Fish: A Systematic Review. *Process Safety and Environmental Protection* **2021**, *152*, 14–24. <https://doi.org/10.1016/J.PSEP.2021.05.020>.
  - (28) Bechshoft, T.; Wright, A. J.; Styrisshave, B.; Houser, D. Measuring and Validating Concentrations of Steroid Hormones in the Skin of Bottlenose Dolphins (*Tursiops Truncatus*). *Conservation Physiology* **2020**, *8* (1). <https://doi.org/10.1093/CONPHYS/COAA032>.
  - (29) Ospina-Álvarez, N.; Piferrer, F. Temperature-Dependent Sex Determination in Fish Revisited: Prevalence, a Single Sex Ratio Response Pattern, and Possible Effects of Climate Change. *PLOS ONE* **2008**, *3* (7), e2837. <https://doi.org/10.1371/JOURNAL.PONE.0002837>.
  - (30) Munday, P. L.; Buston, P. M.; Warner, R. R. Diversity and Flexibility of Sex-Change Strategies in Animals. *Trends in ecology & evolution* **2006**, *21* (2), 89–95. <https://doi.org/10.1016/J.TREE.2005.10.020>.
  - (31) Guiguen, Y.; Fostier, A.; Piferrer, F.; Chang, C. F. Ovarian Aromatase and Estrogens: A Pivotal Role for Gonadal Sex Differentiation and Sex Change in Fish. *General and comparative endocrinology* **2010**, *165* (3), 352–366. <https://doi.org/10.1016/J.YGCEN.2009.03.002>.
  - (32) Castanheira, M. F.; Conceição, L. E. C.; Millot, S.; Rey, S.; Bégout, M. L.; Damsgård, B.; Kristiansen, T.; Höglund, E.; Øverli, Ø.; Martins, C. I. M. Coping Styles in Farmed Fish: Consequences for Aquaculture. *Reviews in Aquaculture* **2017**, *9* (1), 23–41. <https://doi.org/10.1111/RAQ.12100>.
  - (33) Atteke, C.; Vetillard, A.; Fostier, A.; Garnier, D.-H.; Jegou, P.; Bailhache, T. Effects of Progesterone and Estradiol on the Repro-Ductive Axis in Immature Diploid and Triploid Rainbow Trout. *Comp. Biochem. Physiol. A Mol. Integr. Physiol* **2003**, *134*, 693–705.
  - (34) Robeck, T. R.; Steinman, K. J.; Parry, C. B.; Gomez, F. M.; Jen-sen, E. D. Comparisons of Serum Progesterone and Progesterone Concentrations in Normal and Abnormal Bottlenose Dolphin (*Tursiops Truncatus*) Pregnancies. *Front. Mar. Sci* **2021**, *8*, 630–563.
  - (35) Orlando, E. F.; Ellestad, L. E.; Sources. Concentrations, and Exposure Effects of Environmental Gestagens on Fish and Other Aquatic Wildlife, with an Emphasis on Reproduction. *Gen Comp Endocrinol* **2014**, *203*, 241–249.
  - (36) Korpela, J.; Suzuki, H.; Matsumoto, S.; Mizutani, Y.; Samejima, M.; Maekawa, T.; Nakai, J.; Yoda, K. Machine Learning Enables Improved Runtime and Precision for Bio-Loggers on Seabirds. *Communications Biology* **2020**, *3* (1), 1–9. <https://doi.org/10.1038/s42003-020-01356-8>.
  - (37) Sempionatto, J. R.; Lin, M.; Yin, L.; De la paz, E.; Pei, K.; Sonsa-ard, T.; de Loyola Silva, A. N.; Khorshed, A. A.; Zhang, F.; Tostado, N.; Xu, S.; Wang, J. An Epidermal Patch for the Simultaneous Monitoring of Haemodynamic and Metabolic Biomarkers. *Nature Biomedical Engineering* **2021**, *5* (7), 737–748. <https://doi.org/10.1038/s41551-021-00685-1>.
  - (38) Geng, Z.; Zhang, X.; Fan, Z.; Lv, X.; Su, Y.; Chen, H. Recent Progress in Optical Biosensors Based on Smartphone Platforms. *Sensors* **2017**, *Vol. 17*, Page 2449 **2017**, *17* (11), 2449. <https://doi.org/10.3390/S17112449>.
  - (39) O’Connell, M. J.; Bachilo, S. H.; Huffman, C. B.; Moore, V. C.; Strano, M. S.; Haroz, E. H.; Rialon, K. L.; Boul, P. J.; Noon, W. H.; Kittrell, C.; Ma, J.; Hauge, R. H.; Weisman, R. B.; Smalley, R. E. Band Gap Fluorescence from Individual Single-Walled Carbon Nanotubes. *Science* **2002**, *297* (5581), 593–596. <https://doi.org/10.1126/SCIENCE.1072631/ASSET/67B598C0-C187-4745-B979-D284272E029E/ASSETS/GRAPHIC/SE2920711004.JPEG>.
  - (40) Hong, G.; Diao, S.; Chang, J.; Antaris, A. L.; Chen, C.; Zhang, B.; Zhao, S.; Atochin, D. N.; Huang, P. L.; Andreasson, K. I.; Kuo, C. J.; Dai, H. Through-Skull Fluorescence Imaging of the Brain in a New near-Infrared Window. *Nature Photonics* **2014**, *8* (9), 723–730. <https://doi.org/10.1038/nphoton.2014.166>.
  - (41) Beyene, A. G.; Delevich, K.; Del Bonis-O’Donnell, J. T.; Piekarski, D. J.; Lin, W. C.; Wren Thomas, A.; Yang, S. J.; Kosillo, P.; Yang, D.; Prounis, G. S.; Wilbrecht, L.; Landry, M. P. Imaging Striatal Dopamine Release Using a Nongenetically Encoded near Infrared Fluorescent Catecholamine Nanosensor. *Science Advances* **2019**, *5* (7). [https://doi.org/10.1126/SCIADV.AAW3108/SUPPL\\_FILE/A AW3108\\_SM.PDF](https://doi.org/10.1126/SCIADV.AAW3108/SUPPL_FILE/A AW3108_SM.PDF).
  - (42) Kruss, S.; Landry, M. P.; Vander Ende, E.; Lima, B. M. A. a; Reuel, N. F.; Zhang, J.; Nelson, J.; Mu, B.; Hilmer, A.; Strano, M. Neurotransmitter Detection Using Corona Phase Molecular Recognition on Fluorescent Single-Walled Carbon Nanotube Sensors. *Journal of the American Chemical Society* **2014**, *136* (2), 713–724. <https://doi.org/10.1021/ja410433b>.

- (43) Bisker, G.; Dong, J.; Park, H. D.; Iverson, N. M.; Ahn, J.; Nelson, J. T.; Landry, M. P.; Kruss, S.; Strano, M. S. Protein-Targeted Corona Phase Molecular Recognition. *Nature Communications* **2016**, *7*, 1–14. <https://doi.org/10.1038/ncomms10241>.
- (44) Jin, X.; Lee, M. A.; Gong, X.; Koman, V. B.; Lundberg, D. J.; Wang, S.; Bakh, N. A.; Park, M.; Dong, J. I.; Kozawa, D.; Cho, S. Y.; Strano, M. S. Corona Phase Molecular Recognition of the Interleukin-6 (IL-6) Family of Cytokines Using nIR Fluorescent Single-Walled Carbon Nanotubes. *ACS Applied Nano Materials* **2023**, *6* (11), 9791–9804. <https://doi.org/10.1021/acsanm.3c01525>.
- (45) Lee, M. A.; Wang, S.; Jin, X.; Bakh, N. A.; Nguyen, F. T.; Dong, J.; Silmore, K. S.; Gong, X.; Pham, C.; Jones, K. K.; Muthupalani, S.; Bisker, G.; Son, M.; Strano, M. S. Implantable Nanosensors for Human Steroid Hormone Sensing In Vivo Using a Self-Templating Corona Phase Molecular Recognition. *Advanced Healthcare Materials* **2020**, *9* (21), 2000429. <https://doi.org/10.1002/adhm.202000429>.
- (46) Zhang, J.; Landry, M. P.; Barone, P. W.; Kim, J.-H.; Lin, S.; Ulissi, Z. W.; Lin, D.; Mu, B.; Boghossian, A. A.; Hilmer, A. J.; Rwei, A.; Hinckley, A. C.; Kruss, S.; Shandell, M. A.; Nair, N.; Blake, S.; Şen, F.; Şen, S.; Croy, R. G.; Li, D.; Yum, K.; Ahn, J.-H.; Jin, H.; Heller, D. A.; Essigmann, J. M.; Blankschtein, D.; Strano, M. S. Molecular Recognition Using Corona Phase Complexes Made of Synthetic Polymers Adsorbed on Carbon Nanotubes. *Nat. Nanotechnol* **2013**, *8* (12), 959.
- (47) Lowe, C. L.; Hunt, K. E.; Rogers, M. C.; Neilson, J. L.; Robbins, J.; Gabriele, C. M.; Teerlink, S. S.; Seton, R.; Buck, C. L. Multi-Year Progesterone Profiles During Pregnancy in Baleen of Humpback Whales (Megaptera Novaeangliae. *Conserv Physiol* **2021**, *9*, 059 1–14.
- (48) Robeck, T. R.; Steinman, K. J.; O'Brien, J. K. Characterization and Longitudinal Monitoring of Serum Androgens and Glu-Cocorticoids during Normal Pregnancy in the Killer Whale (Or-Cinus Orca. *Gen. Comp. Endocrinol* **2017**, *247*, 116–129.
- (49) Pietraszek, J.; Atkinson, S. Concentrations of Estrone Sulfate and Progesterone in Plasma and Saliva, Vaginal Cytology, and Bioelectric Impedance during the Estrous Cycle of the Ha-Waiian Monk Seal (Monachus Schauinslandi. *Mar. Mammal Sci* **1994**, *10* (4), 430–441.
- (50) Gesto, M.; Hernández, J.; López-Patiño, M. A.; Soengas, J. L.; Míguez, J. M. Is Gill Cortisol Concentration a Good Acute Stress Indicator in Fish? A Study in Rainbow Trout and Zebrafish. *Comparative Biochemistry and Physiology Part A: Molecular & Integrative Physiology* **2015**, *188*, 65–69.
- (51) Nouri, M.-Z.; Kroll, K. J.; Webb, M.; Denslow, N. D. Quantification of Steroid Hormones in Low Volume Plasma and Tissue Homogenates of Fish Using LC-MS/MS. *General and Comparative Endocrinology* **2020**, *296*, 113543.
- (52) Khatun, P.; Saha, P.; Islam, M. Z.; Islam, A.; Islam, M. A.; Islam, P. The Reality of the Use of Growth Hormones in Fish. *Current Research in Food Science* **2024**, *8*, 100709.



## Table of Contents Figure



## Supporting Information

### A Nanosensor Platform for Biologging in Marine Animals

Xiaojia Jin<sup>1</sup>, Ali A. Alizadehmojarad<sup>1</sup>, Volodymyr B. Koman<sup>1</sup>, Gabriel Sánchez-Velázquez<sup>1</sup>, Manki Son<sup>1</sup>, Rory Wilson<sup>2</sup>, Mark Meekan<sup>3</sup>, Carlos M. Duarte<sup>4</sup>, and Michael S. Strano<sup>1,\*</sup>

<sup>1</sup> 77 Massachusetts Ave., Department of Chemical Engineering, Massachusetts Institute of Technology, Cambridge, MA, 02139, USA

<sup>2</sup> Biosciences, College of Science, Swansea University, Singleton Park, Swansea SA2 8PP, United Kingdom

<sup>3</sup> Australian Institute of Marine Science, the Indian Ocean Marine Research Centre (IOMRC), The University of Western Australia (M470), 35 Stirling Highway, 6009 Perth, Australia

<sup>4</sup> Red Sea Research Center, Division of Biological and Environmental Sciences and Engineering, King Abdullah University of Science and Technology, Thuwal 23955-6900, Saudi Arabia

\*Corresponding author's email address: [strano@mit.edu](mailto:strano@mit.edu)

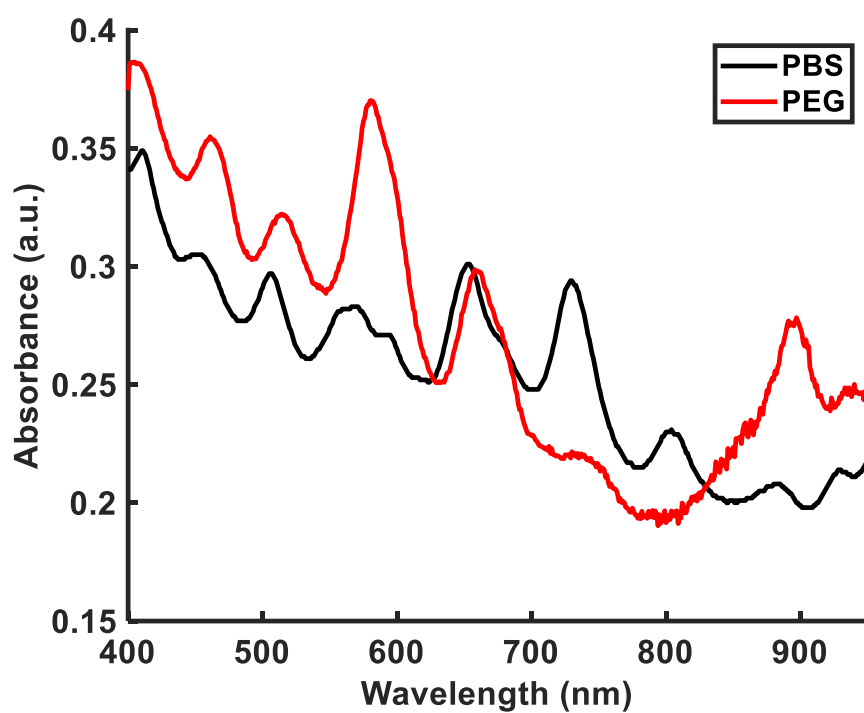
Table of Contents:

**Figure S1.** UV-Vis absorption spectrum of the progesterone sensor in buffer condition and in PEGDA hydrogel solution before crosslinking.

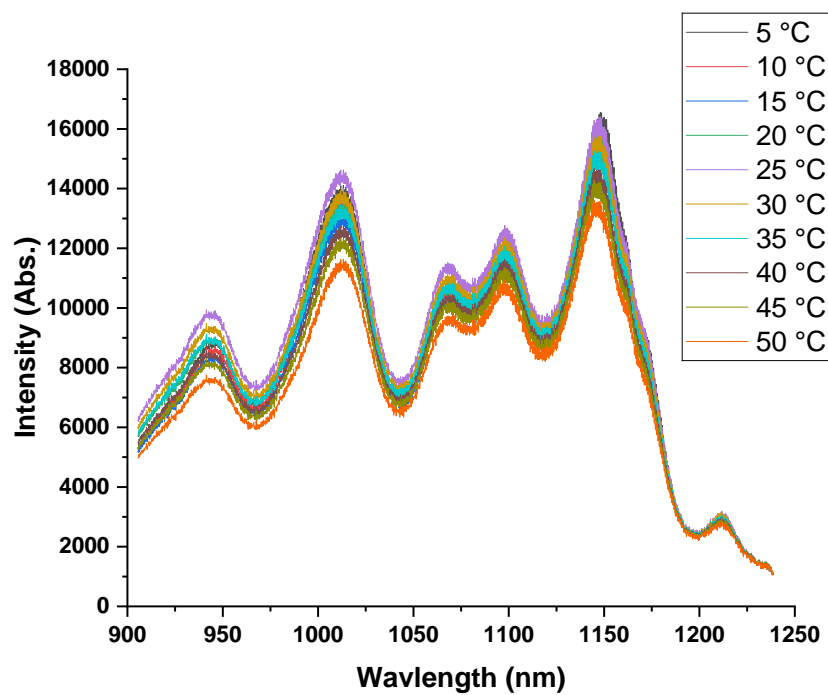
**Figure S2.** Raw fluorescence emission spectra of the nanosensor at different solution temperature.

**Table S1.** Photodiode specifications used for the study

**Table S2.** LED specifications used for the study






**Figure S1.** UV-Vis absorption spectrum of the progesterone sensor in buffer condition and in PEGDA hydrogel solution before crosslinking.



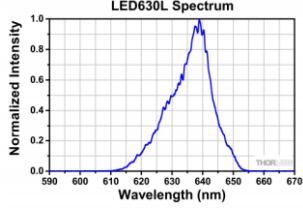
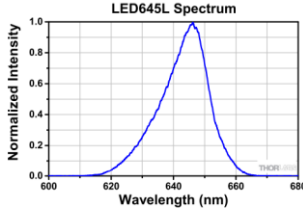
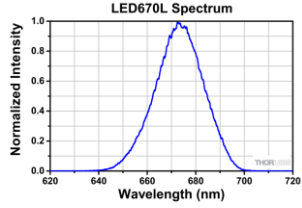
**Figure S2.** Raw fluorescence emission spectra of the nanosensor at different solution temperature.

**Table S1.** Photodiode specifications used for the study

Photodiode	FGA21	FGA10	FDGA05
Image			
Wavelength range (nm)	800 - 1700	900 – 1700	800 – 1700
Peak wavelength (nm)	1590	1550	1550
Active area (mm <sup>2</sup> )	3.1	0.79	0.196
Rise / Fall time	25 ns / 25 ns	10 ns / 10 ns	2.5 ns / 2.5 ns
Responsivity	1.04 A/W	1.05 A/W	0.95 A/W



**Table S2.** LED specifications used for the study

LED	LED 630L	LED 645L	LED 670L
Spreading angle (deg)	22	20	22
Emission Spectrum			
L-I-V Characteristic	